Testing galaxy formation models with galaxy stellar mass functions

S.H. Lim[1]*, H.J. Mo[1,2], Ting-Wen Lan[3,4] and Brice Ménard[3,4]

[1] *Department of Astronomy, University of Massachusetts, Amherst MA 01003-9305, USA*
[2] *Physics Department and Center for Astrophysics, Tsinghua University, Beijing 10084, China*
[3] *Kavli IPMU (WPI), UTIAS, The University of Tokyo, Kashiwa, Chiba 277-8583, Japan*
[4] *Department of Physics & Astronomy, Johns Hopkins University, Baltimore MD 21218, USA*

ABSTRACT

We compare predictions of a number of empirical models and numerical simulations of galaxy formation to the conditional stellar mass functions (CSMF) of galaxies in groups of different masses obtained recently by Lan et al. to test how well different models accommodate the data. The observational data clearly prefer a model in which star formation in low-mass halos changes behavior at a characteristic redshift $z_c \sim 2$. There is also tentative evidence that this characteristic redshift depends on environment, becoming $z_c \sim 4$ in regions that eventually evolve into rich clusters of galaxies. The constrained model is used to understand how galaxies form and evolve in dark matter halos, and to make predictions for other statistical properties of the galaxy population, such as the stellar mass functions of galaxies at high z, the star formation and stellar mass assembly histories in dark matter halos. A comparison of our model predictions with those of other empirical models shows that different models can make vastly different predictions, even though all of them are tuned to match the observed stellar mass functions of galaxies.

Key words: methods: statistical – galaxies: formation – galaxies: evolution – galaxies: haloes.

1 INTRODUCTION

In the current paradigm of structure formation within the Λ cold dark matter (ΛCDM) framework, initial small fluctuations in the cosmic density field are amplified by gravitational instability, eventually forming highly nonlinear structures called dark matter halos (see Mo et al. (2010) for a review). Galaxies then form at the centers of the gravitational potential wells of the dark matter halos by radiative cooling and condensations of baryonic gas (e.g. White & Rees 1978; Fall & Efstathiou 1980; Mo et al. 1998). In order to reproduce the observed stellar mass function of galaxies in the CDM scenario, however, star formation in dark matter halos has to be inefficient (e.g. Yang et al. 2003), and various feedback processes have been proposed to suppress the star formation efficiency in dark matter halos.

In this framework, therefore, galaxy formation and evolution are governed by a number of physical processes which, in turn, are characterized by a number of characteristic scales. First, cosmological N-body simulations have shown that the assembly histories of dark matter halos in general consist of two distinctive phases: an earlier phase of fast mass acquisition during which the potential well of a halo deepens rapidly with time, and a later phase of slow accretion, with a time scale longer than the Hubble time (e.g. Zhao et al. 2003). Zhao et al. (2009) found that the two phases are separated at a time when a halo obtains about $\sim 4\%$ of its final mass (see also van den Bosch et al. 2014). Second, hydrodynamical simulations have demonstrated that radiative cooling is effective in halos with masses smaller than $M_h \sim 6 \times 10^{11} M_\odot$, so that the accretion rate of cold gas into galaxies is determined by the halo mass accretion rate, independent of radiative cooing (e.g. Kereš et al. 2005, 2009). Above this mass scale, on the other hand, radiative cooling is ineffective, so that the cold gas accretion is delayed by the cooling time scale. For massive halos with masses above $10^{13} M_\odot$, a significant fraction of the baryonic gas is expected to be in the hot halo in the absence of a heating source. Third, supernova feedback from star formation is believed to be effective for halos with masses below $\sim 10^{11} M_\odot$ (e.g. Dekel & Silk 1986; Somerville et al. 2008; Lu et al. 2012). Finally AGN feedback from accreting super-massive black holes has been proposed as a mechanism to suppress star for-

* E-mail: slim@astro.umass.edu

mation in massive halos, with masses above $M_h \sim 10^{13}\mathrm{M}_\odot$ (e.g. Ferrarese & Merritt 2000; McConnell et al. 2011).

A number of approaches have been adopted to explore the physical processes that govern galaxy formation and evolution, and to facilitate comparisons between theory and observation. The first is hydrodynamical simulation that includes both dark matter and baryonic components (e.g. Dubois et al. 2014; Khandai et al. 2015; Vogelsberger et al. 2014; Schaye et al. 2015). However, due to limited resolution and subgrid implementations of some key processes, the results obtained from such simulations are still questionable, even though they can match some observational data (e.g. Governato et al. 2004, 2010; Okamoto et al. 2005; Guedes et al. 2011). Furthermore, high resolution hydrodynamical simulations are computationally expensive, which prohibits the explorations of a large parameter space. Because of this, an alternative approach, the semi-analytic model (SAM) of galaxy formation, has been developed (e.g. White & Frenk 1991; Kauffmann et al. 1999; Kang et al. 2005; Bower et al. 2006; Croton et al. 2006; Somerville et al. 2008; Guo et al. 2011; Lu et al. 2011). The SAM approach combines halo merger histories, obtained either from dark-matter only simulations or from analytical models, with gas and star formation processes using parametrized functions that describe the underlying physical processes. This approach is computationally inexpensive, allowing one to investigate a large set of different models. However, since all the physical processes are approximated with simple empirical functions, the reliability and accuracy of this approach needs to be checked. More recently, a third approach has been adopted to understand how galaxies form and evolve in the cosmic density field. The goal of this approach is to establish the connections between galaxies and dark matter halos through an empirical approach, using observational data as constraints. Models developed along this line include the halo occupation distribution (HOD; e.g. Jing et al. 1998; Peacock & Smith 2000; White 2001; Berlind & Weinberg 2002; Bullock et al. 2002; Zehavi et al. 2004, 2011), the conditional luminosity function (CLF; Yang et al. 2003, 2012; van den Bosch et al. 2003), the halo abundance matching model (HAM; Kravtsov et al. 2004; Vale & Ostriker 2004, 2006; Conroy et al. 2006; Behroozi et al. 2010; Guo et al. 2010; Moster et al. 2010; Reddick et al. 2013), and the halo-based empirical model (Lu et al. 2014, 2015).

To a certain degree, both the SAM and empirical approaches are methods to summarize observational data in terms of model parameters characterizing the galaxy-halo connections. Much progress has been made recently in this area. Using the CLF model and constraints of the observed luminosity function and correlation function of galaxies, Yang et al. (2003) found a characteristic halo mass scale, $\sim 10^{12}\mathrm{M}_\odot$, in the relationship between galaxy luminosity/stellar mass and halo mass relation, suggesting that star formation efficiency declines rapidly toward both the higher and lower mass ends. With the use of galaxy groups selected from the 2dF (Yang et al. 2005) and SDSS (Yang et al. 2007), Yang et al. (2005) found a similar mass scale from the observed galaxy luminosity/stellar mass - halo mass relations obtained directly from galaxy groups. In particular, Yang et al. (2005) suggested the existence of another characteristic mass scale, $\sim 10^{11}\mathrm{M}_\odot$, where the galaxy luminosity-halo mass relation may change its behavior. Similar results have

since been obtained at higher z with the use of the observed luminosity/stellar mass functions of galaxies. In particular, the presence of the mass scale at $\sim 10^{12}\mathrm{M}_\odot$ seems to extend to higher z without showing strong evolution (Moster et al. 2010; Behroozi et al. 2013; Guo et al. 2010; Yang et al. 2012).

More recently, Lu et al. (2014, 2015) developed a halo-based empirical model to follow the star formation and stellar mass assembly histories of galaxies in dark matter halos. In particular, they used the observed conditional luminosity functions of cluster galaxies obtained by Popesso et al. (2006) as an constraint in addition to the field stellar mass functions at different redshifts. They found that the observational data require two additional characteristic scales, a characteristic redshift, $z \sim 2-3$, and a corresponding mass scale at $10^{11}\mathrm{M}_\odot$, below which star formation changes behavior at the characteristic redshift. These results clearly demonstrate that the observed conditional luminosity/stellar mass function of galaxies in clusters can provide important information about galaxy formation and evolution at high redshift. However, since clusters of galaxies only contain a small fraction of the total galaxy population, the results may be affected by some environmental effects that are specific only to clusters of galaxies.

Using the galaxy groups of Yang et al. (2007) combined with galaxies in the SDSS photometric catalogue, Lan et al. (2016) have recently measured the conditional luminosity/stellar mass functions (hereafter CSMFs) that cover four orders of magnitude in galaxy luminosity, and three orders of magnitude in halo mass, from $\sim 10^{12}$ to $10^{15}\mathrm{M}_\odot$. They found a characteristic luminosity scale, $L \sim 10^9 L_\odot$, below which the slope of the CSMF becomes systematically steeper, and that this trend is present for all halo masses. This ubiquitous faint-end upturn suggests that it is formation, rather than cluster-specific environmental effect, that plays the dominating role in regulating the stellar masses of faint satellites. Clearly, these observational results will provide new constraints on models.

This paper consists of two parts. First, we use the new CSMFs to update the empirical model of Lu et al. (2014, 2015) and show that there is only marginal difference between the original model and the updated model. Second, we compare model predictions from empirical models and numerical simulations to the CSMFs of Lan et al. to test how well different models accommodate the new data. We will show that, among all the models considered, only the Lu et al. (2014, 2015) model can match the observational data reasonably well. Also, we present predictions of the different models for other statistical properties of the galaxy population.

The organization of this paper is as follows. Section 2 describes the empirical models to be tested and two recent numerical simulations, Illustris (Vogelsberger et al. 2014) and EAGLE (Schaye et al. 2015), to be compared. In Section 3, we describe the observational data that are used in our analysis, and present comparisons of the empirical models and the simulations with them. In Section 4, we present a more detailed comparison of the model predictions in star formation rate, stellar mass - halo mass relation, mass assembly history, and stellar mass function for high redshifts. Finally, we summarize and discuss our results in Section 5.

Table 1. A list of the models and the simulations.

Model / Simulation	Reference
Y12	Yang et al. (2012)
M13	Moster et al. (2013)
B13	Behroozi et al. (2013)
L15	Lu et al. (2015)
L15-U	this work
Illustris	Vogelsberger et al. (2014)
EAGLE	Schaye et al. (2015)

2 MODELS

In this paper we select a number of popular empirical models and two recent hydrodynamical simulations to test against observational data. Here we describe these models and simulations briefly. Table 1 lists the models and the simulations that we test. Readers are referred to the original papers for details.

2.1 Empirical models

One of the simplest way to link galaxies to their dark matter halo/subhalo population is to use halo abundance matching (e.g. Mo et al. 1999). This approach assumes a monotonic relation between halo mass and galaxy stellar mass. Satellite galaxies observed at a given redshift were all once central galaxies before they were accreted onto larger halos. Since satellites are expected to evolve differently due to environmental effects such as tidal stripping and ram pressure stripping, many abundance matching models apply a monotonic relation between galaxy stellar mass and halo mass at the time when a halo first became a subhalo, instead of at the time of observation. Most of previous investigations make the assumption that the halo mass - galaxy mass relation is independent of when a sub-halo is accreted into its host (e.g. Vale & Ostriker 2004, 2006; Conroy et al. 2006; Behroozi et al. 2010; Guo et al. 2010; Moster et al. 2010). With this assumption, at a given redshift, halos of a given mass are therefore always linked to galaxies of the same stellar mass. However, it was found that applying this method to different redshifts actually leads to different stellar mass - halo mass relation (e.g. Conroy et al. 2006), suggesting that the method implemented in this way is not self-consistent. As an improvement, models have been developed in which the galaxy-halo relation is allowed to depend on both halo mass (defined e.g. at the time when a halo first becomes a sub-halo) and the time when a halo becomes a sub-halo. We test four models in this category, by Yang et al. (2012), Moster et al. (2013), Behroozi et al. (2013), and Lu et al. (2015), respectively.

2.1.1 Yang et al. model

The model of Yang et al. (2012) (Y12, hereafter) takes the same functional form as that proposed in Yang et al. (2003)

for the halo mass - galaxy luminosity/stellar mass relation:

$$\frac{M_*}{M_h} = N \left[\left(\frac{M_h}{M_1} \right)^{-\beta} + \left(\frac{M_h}{M_1} \right)^{\gamma} \right]^{-1}. \tag{1}$$

This is basically a double power law specified by two asymptotic slopes, β and γ, describing the low- and high-mass end behaviors, respectively, and by a characteristic mass scale M_1 where the transition between the two power laws occurs, and with N being an overall amplitude. The four free parameters were assumed to be redshift dependent and the dependencies were modeled by simple functions. The above relation was used to assign stellar masses to halos at different redshifts. They adopted the halo mass function of Sheth et al. (2001) to model the halo population. For sub-halos, the model of Yang et al. (2011) was used to follow both the mass function and the distribution in the accretion time (the time when a halo first becomes a subhalo). A stellar mass is assigned to a sub-halo at the time of accretion according to its mass at that time using equation (1). The subsequent evolution of the satellite associated with a sub-halo was followed according to its orbit determined through a dynamical friction model. The model parameters were then obtained by fitting the model predictions to the observed stellar mass functions (SMFs) of galaxies from $z = 0$ to 4, and the correlation function of $z \sim 0$ galaxies as a function of galaxy luminosity/stellar mass.

2.1.2 Moster et al. model

Moster et al. (2013) (M13) adopted a similar double power-law for the stellar mass - halo mass relation as described by equation (1), and simple functional forms to describe the redshift dependencies of the model parameters. They applied the relation to halos and sub-halos obtained from N-body simulations. Individual halos and sub-halos are matched and traced across different snapshots (i.e. different redshifts), so that merger trees are generated to track their evolutions. Galaxies hosted at the centers of halos and sub-halos were referred to as centrals and satellites, respectively. For centrals, the stellar masses were given by the stellar mass - halo mass relation using the redshift and halo mass at the snapshot in question. For satellites, the stellar masses were obtained by applying the stellar mass - halo mass relation at the redshift when their halos first became sub-halos using their halo masses at this redshift, as in Y12. The stellar mass of a satellite was assumed to remain unchanged in the subsequent evolution. Some uncertainties in the stellar mass - halo mass relation were taken into account. Model parameters characterizing the stellar mass - halo mass relation were then tuned to match a set of observed SMFs from $z = 0$ to 4.

2.1.3 Berhoozi et al. model

The approach adopted by Behroozi et al. (2013) (B13) was similar to those of Y12 and M13, but the stellar mass - halo mass relation assumed was more complicated and was designed in part to reproduce the observed SMFs at the faint ends. Here again, halo merger trees extracted from N-body simulations were used to trace the formation of dark matter halos. As in Y12 and M13, they applied their stellar mass -

halo mass relation to 'infall' mass at the time of accretion to assign stellar masses to subhalos. Subsequent stellar mass loss of satellites after their accretion into their host halos was also taken into account. Finally, they used the observed SMFs at $z = 0$ - 8, as well as the cosmic star formation rates and specific star formation rates, to constrain their model parameters.

2.1.4 Lu et al. model

The Lu et al. (2014, 2015) model (hereafter L15) was based on the star formation rate (SFR) - halo mass relation as a function of redshift:

$$\dot{M}_*(M_h, z) = \varepsilon \frac{f_b M_h}{\tau}(x+1)^\alpha \left(\frac{x+R}{x+1}\right)^\beta \left(\frac{x}{x+R}\right)^\gamma \quad (2)$$

where $f_b = \Omega_{b,0}/\Omega_{m,0}$, $\tau = [10H_0(1+z)^{3/2}]^{-1}$ approximates the dynamical time of halos, $x \equiv M_h/M_c$, with M_c being a characteristic mass scale and R is parameter of $0 \leqslant R \leqslant 1$. Thus, $\dot{M}_*/M_h \propto M_h^{\{\alpha,\beta,\gamma\}}$ for $\{M_h \gg M_c, RM_c < M_h < M_c$, and $M_h \ll RM_c\}$, respectively. This relation is applied only to central galaxies. After a galaxy becomes a satellite, Lu et al. assumed that it moves on an orbit determined by its initial energy and orbital angular momentum together with dynamical friction. A satellite galaxy is assumed to merge with the central galaxy once it sinks to the center of the halo. At this time, it adds a fraction (treated as a free parameter, f_{sc}) of its mass to the central galaxy, and the rest is assumed to become halo stars. The SFRs in satellites were modeled with a simple exponential model,

$$\dot{M}_{*,sat} \propto \exp\left[-\frac{t - t_{acc}}{\tau_s}\right] \quad (3)$$

where t_{acc} is the time when the galaxy becomes a satellite, and $\tau_s = \tau_{s,0} \exp\left[-M_*/M_{*,c}\right]$ is adopted to reflect halo mass dependence of the time scale, with $\tau_{s,0}$ and $M_{*,c}$ being free parameters. The stellar mass in a galaxy is then obtained by integrating the SFR over time, taking into account mass loss due to stellar evolution. Lu et al. used halo merger trees generated with the algorithm developed by Parkinson et al. (2008), which is based on the extended Press-Schechter formalism calibrated with N-body simulations.

Lu et al. adjusted both their functional forms and free parameters to match the SMFs at $0 < z < 4$ and the CSMFs of galaxies in clusters of galaxies as given by Popesso et al. (2006). They found that the model assuming all the parameters to be independent of redshift is not able to match the observed SMFs at high redshift. They therefore extended their model by allowing α to change with redshift as $\alpha = \alpha_0(1+z)^{\alpha'}$. This model was referred to as Model II in Lu et al.. Model II was found to be able to describe all the stellar mass functions (SMFs) at both low and high redshifts, but fails to match the faint-end upturn in the CSMF of cluster galaxies. Because of this, Lu et al. extended their model once more by allowing the parameter γ, which dictates the SFR in low-mass halos, to depend on redshift:

$$\gamma = \gamma_a \qquad \text{if } z \leqslant z_c$$
$$= (\gamma_a - \gamma_b)\left(\frac{1+z}{1+z_c}\right)^{\gamma'} \qquad \text{if } z > z_c$$

In this model, referred to as Model III by Lu et al., $\gamma \to \gamma_b$ at $z \gg z_c$, and the free parameter, γ', controls how rapidly
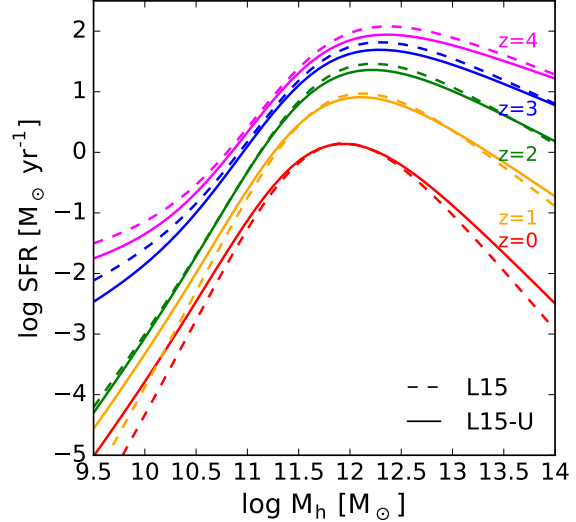
Figure 1. The average star formation rate of central galaxies as a function of halo mass at different redshifts as predicted by the original L15 model (dashed lines) and the L15-U model (solid lines).

the transition to γ_b occurs above the characteristic redshift z_c. This Model III was found to be able to fit both the SMFs at different redshifts and the CSMF of cluster galaxies simultaneously.

2.1.5 Updating the parameters of the L15 model

Instead of using the model parameters of Lu et al., we use only the observed CSMFs as constraints to update the model parameters. We use the MULTINEST method developed by Feroz et al. (2009), which makes use of the nested sampling algorithm of Skilling et al. (2006), to compute the posterior distribution of the model parameters. The MULTINEST is found to yield practically the same results as the traditional MCMC method but with ~ 10 times smaller number of likelihood calculations for the problem concerned here. The reader is referred to the original papers for details.

Table 2 compares the updated parameters with the model parameters of Lu et al. The average star formation rates predicted with the updated parameters at various redshifts are very similar to those obtained by L15, as shown in Figure 1. We also found that the differences in the two parameter sets result only in marginal changes in the CSMFs in that the updated model (hereafter L15-U) predicts slightly flatter slopes at the faint-ends for massive haloes. This is owing to the fact that the Lan et al. CLFs have shallower faint-end slopes for massive halos than the cluster galaxy luminosity function used by L15. The marginal difference between the two parameter sets demonstrates that the low-z CSMFs alone can constrain models in a similar way as the field SMFs at different redshifts. Furthermore, as we will see in §4), they also contain information about the low-mass end of the SMF at high z, where direct observations are still uncertain. We use L15-U to present results throughout this paper.

Table 2. A list of the model parameters. The medians and the standard deviations are presented.

parameters	L15	L15-U
α_0	-3.0 ± 1.0	-2.7 ± 0.79
α'	-0.36 ± 0.16	-0.32 ± 0.21
β	3.7 ± 0.73	3.5 ± 1.0
γ_a	2.0 ± 0.55	1.3 ± 0.69
γ_b	-0.84 ± 0.14	-1.1 ± 0.21
γ'	-4.4 ± 0.52	-3.1 ± 0.88
z_c	1.8 ± 0.31	2.0 ± 0.28
$\log_{10} M_c$	1.6 ± 0.15	1.6 ± 0.11
$\log_{10} R$	-0.86 ± 0.18	-0.92 ± 0.20
ε	0.20 ± 0.29	0.050 ± 0.11
$\log_{10} H_0 \tau_{s,0}$	-0.90 ± 0.16	-0.85 ± 0.11
$\log_{10} M_{*,c}$	0.34 ± 0.28	0.18 ± 0.19
f_{sc}	0.44 ± 0.22	0.52 ± 0.15

2.1.6 Need for a more extended model family?

As mentioned above, L15 assumed the characteristic redshift, z_c, the redshift at which the SFR in low mass progenitors changes behavior, to be independent of the host halo mass. However, it is plausible that z_c depends on the host halo mass, because structure formation, and presumably star formation, are expected to occur earlier in regions that correspond to higher mass halos at the present day. Motivated by this, we test a more extended model family in which the characteristic redshift changes with host halo mass at $z = 0$, $M_h(0)$:

$$(1 + z_c) = (1 + z_{c,0}) \left(\frac{M_h(0)}{10^{12} \mathrm{M_\odot}} \right)^\zeta \qquad (4)$$

where ζ controls the halo mass dependence of z_c, and $z_{c,0}$ is z_c for halos of $M_h(0) = 10^{12} \mathrm{M_\odot}$. We use the same CSMFs as used in the earlier subsection to constrain model parameters.

To test if such an extension is necessary, we use the Bayes factor,

$$K = \frac{P(D|M_1)}{P(D|M_2)} = \frac{\int P(D|\theta_1, M_1) P(\theta_1|M_1) d\theta_1}{\int P(D|\theta_2, M_2) P(\theta_2|M_2) d\theta_2}, \qquad (5)$$

where D is a given data set, M_1 and M_2 are two different models, and θ_1 and θ_2 are the parameter space of the models. This factor quantifies the preference of a given data set for one model family over the other. As it integrates over all parameter space of each of the model families, it naturally penalizes over-fitting.

When all the data points of the CSMFs are used as constraints, the Bayes factor between the extended model (the one including ζ) and the original L15 parametrization is given by $2 \ln K \approx 56$, which indicates a strong need for having ζ statistically. The median value of $\zeta \approx 0.064$ thus obtained implies that the characteristic redshift z_c is $z \approx 3.8$ for halos of $M_h(0) = 10^{15} \mathrm{M_\odot}$, in comparison to $z_c \approx 2.1$ for

halos with $M_h(0) = 10^{12} \mathrm{M_\odot}$. This increase of z_c with host halo mass leads to flatter faint-end slopes for massive halos, giving better matches to the faint-ends of the CSMFs for both low-mass and high-mass halos.

It is worth noting, however, that the uncertainties in the stellar mass estimates may change the CSMFs in both the lowest and highest mass ends, where the slopes of the CSMF are steep. As a test, we use only the CSMFs in the range $M_* = [10^8, 10^{11}] \mathrm{M_\odot}$ as the observational constraints. In this case, the models with or without ζ are almost equally favored in terms of the Bayes factor. Given these, we conclude that the original form of the L15 model can still accommodate the new CSMFs, and that the current data are still too uncertain to determine if a more extended model family is required.

2.1.7 Model implementations

We implement the empirical models described above to the dark matter halo population. We use the algorithm developed by Parkinson et al. (2008) to generate halo merger trees and to follow the build-up of dark matter halos. As mentioned above, this algorithm is based on the extended Press-Schechter formalism calibrated with results from N-body simulations. As shown in Jiang & van den Bosch (2014), the predictions of this algorithm match accurately many properties of halo merger trees obtained directly from simulations, including halo mass assembly history, halo merger rate, and sub-halo mass functions.

The empirical models described above also take into account some uncertainties in the observational data and in the model assumptions, such as the intrinsic scatter in the stellar mass - halo mass relation, uncertainties in the stellar population synthesis and dust models, Eddington bias, and errors in redshift measurements. Unfortunately, how these uncertainties change as a function of redshift is poorly established. They are treated differently in different models. M13 adopted constant scatter in the stellar mass - halo mass relation and in the stellar mass estimate, while B13 parametrized the uncertainties as functions of redshift and treated them as a new set of free parameters to be determined in their model fitting. The treatment by Y12 lies in between. In our implementations, we follow each individual model as close as possible.

We use WMAP7 cosmology to obtain the halo mass function, to construct halo merger trees, and to estimate distances from redshifts. We adopt the Chabrier (2003) IMF, the stellar population synthesis model of Bruzual & Charlot (2003) to account for stellar mass loss and to obtain stellar mass function from observations. These assumptions are the same as adopted in the original models, except for Y12 where a Kroupa (2001) IMF was adopted. We correct the stellar masses of Y12 model by a factor of $\sim 1.4/1.7$ to match the IMF we adopt.

2.2 Hydrodynamical simulations

We also test the predictions from two recent high-resolution, cosmological hydrodynamical simulations. The first is Illustris simulation (Nelson et al. 2015), which follows 1820^3 particles for each of the gas and dark matter components in a total volume of $(106.5 \, \mathrm{Mpc})^3$, assuming WMAP9 cosmol-

ogy ($\{\Omega_m, \Omega_\Lambda, h\} = \{0.273, 0.727, 0.704\}$). The other components the simulation traces are stars, stellar wind particles, and super-massive black holes. The simulation starts from $z = 127$ and includes physical processes such as radiative cooling, star formation, and various feedback processes. The free parameters in their model were constrained by using the star formation efficiency obtained from separate simulations that are more accurate in resolving small-scale structures. In our analysis, we use Illustris-1, their flagship simulation that has the highest mass resolution ($1.6 \times 10^6 \mathrm{M}_\odot$ and $6.3 \times 10^6 \mathrm{M}_\odot$ for baryon and dark matter, respectively). To match the set of observations adopted here for model testing, we use the snapshot at $z = 0.03$, which contains a total of $7,647,219$ groups identified by the FoF algorithm. In the simulation, galaxies are defined according to the spatial distribution of stars and stellar wind particles, and the brightness profile fit to them. The simulation assumes the Chabrier (2003) IMF and the stellar population synthesis model of Bruzual & Charlot (2003). As the cosmological parameters of WMAP9 are similar to those of WMAP7, the difference in cosmology is ignored in our analysis. We bin their stellar masses to obtain the stellar mass function (SMF).

Another simulation we use is the Evolution and Assembly of GaLaxies and their Environments (EAGLE; Schaye et al. 2015). EAGLE traces the evolution of gas, stars, dark matter, and massive black holes, and implements physically motivated models for gas cooling, star formation law, stellar and AGN feedback. The free parameters of the feedback models were tuned to match the SMF and black hole mass - stellar mass relation at $z \sim 0$. The simulation starts from $z = 127$ and adopts cosmological parameters from *Planck*: $(\Omega_m, \Omega_\Lambda, h) = (0.307, 0.693, 0.678)$ (Planck 2014). We use their simulation of the largest volume of $(100\mathrm{Mpc})^3$ for our analysis. It contains $\sim 10,000$ galaxies with stellar masses similar to or above that of the Milky Way. Unfortunately, recalibrating their result to account for different cosmology is not trivial, since the impact of changing the parameters to the mass function is highly non-linear in principle. However, the other uncertainties that enter the models or the data must overpower the change in cosmology. We thus do not attempt any recalibration of the simulation results to account for the difference in cosmology. The Chabrier (2003) IMF and the spectral synthesis model of Bruzual & Charlot (2003) were assumed. We bin their stellar masses to get the stellar mass function.

3 COMPARISONS WITH OBSERVATIONAL DATA

In this section, we describe all observational data used for our analyses. These include the stellar mass function (SMF) of the general galaxy population (§3.1), the SMFs separately for central and satellite galaxies (§3.2), and the conditional stellar mass functions (CSMFs) of galaxies (§3.3).

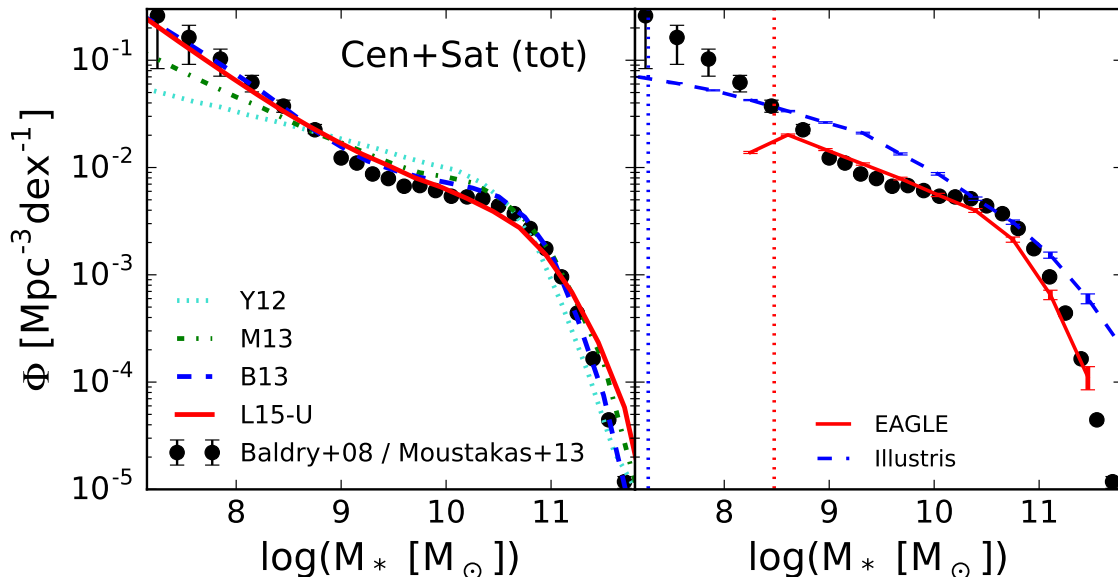## 3.1 The field stellar mass function of galaxies at $z \sim 0$

We use the local ($z \approx 0.1$) SMF obtained from the combination of the results obtained by Baldry et al. (2008) and Moustakas et al. (2013). The data for stellar masses below $M_* \approx 10^9 \mathrm{M}_\odot$ is from Baldry et al., while the data at larger stellar masses is from Moustakas et al.. Here we briefly summarize the methodologies with which the SMFs were computed, and refer the reader to their original papers for details.

Baldry et al. used the New York University Value-Added Galaxy Catalogue (NYU-VAGC; Blanton et al. 2005), which includes $49,968$ galaxies at $z < 0.05$, to construct the local SMF. They adopted the stellar mass estimates from Kauffmann et al. (2003), Gallazzi et al. (2005), and Panter et al. (2007). In the data set we use, the stellar mass estimates are corrected to a Chabrier (2003) IMF.

Moustakas et al. estimated the local SMF using galaxies cross-identified between the Sloan Digital Sky Survey Data Release 7 (SDSS DR7; Abazajian et al. 2009) and the Galaxy Evolution Explorer (GALEX; Martin et al. 2011) Deep Imaging Survey. This results in $\sim 170,000$ galaxies with a total sky coverage of 2505 deg^2. Near-infrared photometry of these galaxies was obtained from the Two Micron All Sky Survey (2MASS; Skrutskie et al. 2006) and the Wide-field Infrared Survey Explorer (WISE; Wright et al. 2010). The photometry in a total of 12 bands (near-UV and far-UV of the GALEX, *ugriz* bands from SDSS model magnitudes, JHK_s magnitudes from the 2MASS, and the integrated photometry at 3.4 and 4.6μm from the WISE All-Sky Data Release) was used to infer the galaxy stellar masses from spectral energy distribution (SED) modelling. More specifically, Moustakas et al. used the Flexible Stellar Population Synthesis model of Conroy et al. (2009), a Chabrier (2003) initial mass function (IMF), exponentially declining star formation histories (SFHs), and the dust attenuation curve of Charlot & Fall (2000), to model the SEDs of individual galaxies. The SMF obtained by Moustakas et al. (2013) is in good agreement with some previous measurements, such as those of Cole et al. (2001), Li & White (2009), and Baldry et al. (2012). See their Appendix B for detailed analyses how variations in the IMF, SFH, spectral synthesis model, and dust attenuation can affect the SMF obtained.

The left panel of Figure 2 compares the predictions of the empirical models with the observed local SMF described above. As one can see, the prediction of the Y12 model is too flat in the low-mass end to match the upturn seen in the observation. This discrepancy owes partly to the simple functional form (a double power-law) they adopted for the stellar mass-halo mass relation, and partly to the SMFs that they used as observational constraints. In fact, Y12 found that the two sets of SMFs at high redshifts that they adopted led to significant differences in the inferred values of model parameters. The results used here are the predictions of 'SMF2' referred in the original paper. The model of M13 also predicts a shallower faint-end slope than the observational data. Similar to Y12, M13 also adopted a simple double power-law form for the stellar mass - halo mass relation, and used a local SMF that has shallower faint-end slope than the one adopted here to constrain their parameters. In contrast, the prediction of B13 matches well the observed SMF, even in the faint end. B13 adopted a rather flexible functional form for the stellar mass - halo mass relation, which is probably required to match the faint-end upturn in the SMF. In addition B13 adopted the combined

Figure 2. The observed stellar mass function of galaxies (data points) in comparison with the predictions of individual empirical models (left) and hydrodynamical simulations (right), as indicated in the panels. The vertical lines in the right panel show the resolution limits of the two simulations, as given in the original papers describing the simulations. The Poisson errors are presented for the simulations.

SMF of Baldry et al. (2008) and Moustakas et al. (2013) as one of their observational constraints, and so the good match between the model prediction and the data is not surprising. The prediction of the L15 model also matches well the observational data. Note that L15 used the SMF of Baldry et al. (2012) as an observational constraint. Their SMF extends only to $10^{8.5} M_\odot$ and so the faint-end upturn is not well represented. The faint-end upturn predicted by L15 is largely due to the CSMF of galaxies in rich clusters, as given by Popesso et al. (2006), they adopted to constrain their model.

The right panel of Figure 2 compares the numerical simulation results with the observational data. Illustris simulation produces too many galaxies in the intermediate mass range as well as in the massive end, but too few low-mass galaxies. The overall shape of the predicted SMF is very different from that of the observed SMF. On the other hand, the prediction of EAGLE simulation matches the observational data reasonably well above the resolution limit. This may not be very surprising, because the free parameters in EAGLE simulation were tuned to match local observations. Unfortunately, the relatively poor mass resolution does not allow us to investigate whether a faint-end upturn is predicted in the simulation.
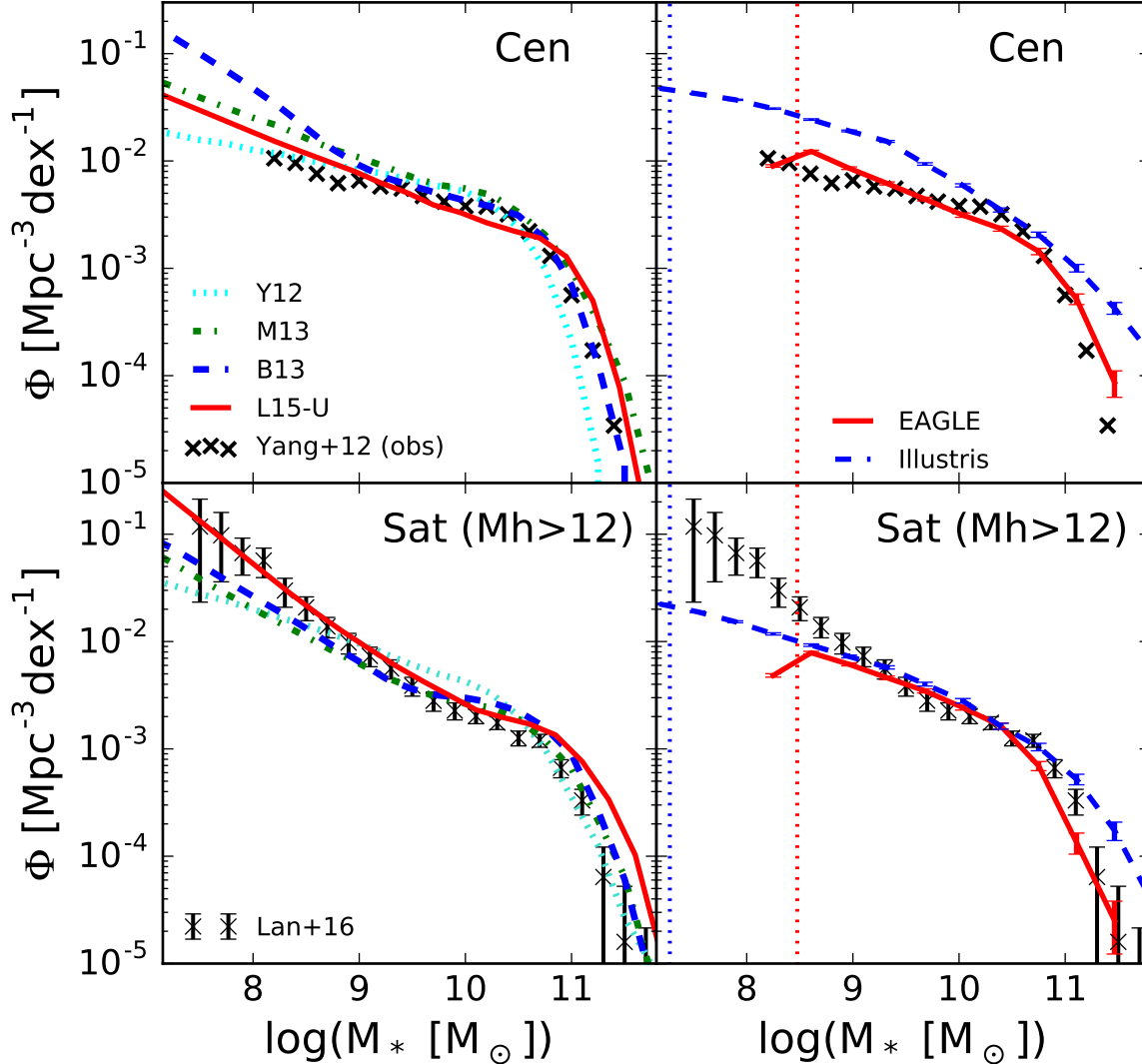
3.2 Central and satellite galaxies

Using the group memberships provided by Yang et al. (2007) group catalog (see next subsection for more details), we can separate galaxies into two populations, centrals and satellites. A central galaxy is defined to be the most massive member in a group, while all other members in a group are called satellites. The CSMFs can then be estimated separately for the centrals and satellites. Formerly the total SMF

can be expressed in terms of these conditional functions as

$$\Phi_{\rm tot}(M_*) = \int_{M_{h,min}}^{\infty} dM_h \; n(M_h) \times \qquad (6)$$
$$\{\Phi_{\rm cen}(M_*|M_h) + \Phi_{\rm sat}(M_*|M_h)\} ,$$

where $\Phi_{\rm cen}(M_*|M_h)$ and $\Phi_{\rm sat}(M_*|M_h)$ are the CSMFs of the centrals and satellites, respectively, in halos of mass M_h, while $n(M_h)$ is the halo mass function, which is the number density of halos of masses between M_h and $M_h + dM_h$. In Lan et al. (2016), the CSMFs are given only for satellites in groups with halo masses above $10^{12} M_\odot$ (see the next subsection for details). The satellite SMF used here is obtained directly from their measurements by summing up the CSMFs of such halos. For central galaxies, we use the results obtained by Yang et al. (2012) from their group catalog. Since the group catalog is based on the SDSS spectroscopic data, the central SMF was measured only for galaxies above $10^8 M_\odot$ (see table 6 in their paper).

The data points in Figure 3 show the SMFs for central and satellite galaxies, respectively. Separating galaxies into centrals and satellites provides more information about the galaxy population than the total SMF alone, and Figure 2 and Figure 3 demonstrate this point clearly. For instance, although the empirical model by B13 (see §2) matches well the faint-end upturn in the observed total SMF, this match is now revealed as due to an excess in the SMF of central galaxies combined with a deficit in the SMF of satellite galaxies. The M13 model has similar problems; it under-estimates the number of satellite galaxies at the low-mass end even more strongly than B13. The Y12 model matches the central SMF reasonably well, but it fails to reproduce the strong upturn in the low-mass end seen in the observed SMF of satellite galaxies. Overall, the L15 model can match both the observed central and satellite SMFs, although some discrepancies in details can still be seen. This match is not trivial,

Figure 3. The observed stellar mass function of central (data points in the upper two panels) and satellite (data points in the lower two panels) galaxies, in comparison with the predictions by individual empirical models (left panels) and gas simulations (right panels), as indicated. The completeness in stellar mass from the observation of centrals is not guaranteed for $M_* < 10^8 M_\odot$. The vertical lines in the right panels show the resolution limits of the two simulations, as given in the original papers describing the simulations.

because these observations were not used as constraints in L15.

The comparisons of the two gas simulations with the observational results are shown in the right two panels of Figure 3. Here we see that the EAGLE simulation matches the observational data reasonably well above its mass resolution limit. Illustris simulation matches the SMF of satellites only in the intermediate mass range; it over-predicts the central SMF over almost the entire mass range, except at the knee of the SMF.

3.3 The conditional stellar mass functions of galaxies in groups

We use the CSMFs obtained by Lan et al. (2016) as our main data set to compare with models. Here we summarize

briefly their methodology and results. Lan et al. used galaxy samples from the NYU-VAGC, which is based on the Sloan Digital Sky Survey Data Release 7 (SDSS DR7; Abazajian et al. 2009). A *K*-correction was applied using the model of Blanton et al. (2003). In order to associate galaxies with clusters/groups of galaxies, they adopted the group catalog of Yang et al. (2007), which was constructed by applying the halo-based group finder developed by Yang et al. (2005) to the SDSS DR7. The group finder assigns galaxies into halos using certain criteria in phase space, and galaxies residing in a common halo are considered to be members of the same group. More specifically, a tentative halo mass is assigned to a tentative group based on the galaxies that have already been assigned to the group, assuming a monotonic relation between the total stellar mass of all assigned members with $M_r < -19.5$ and halo mass. The tentative mass is then used
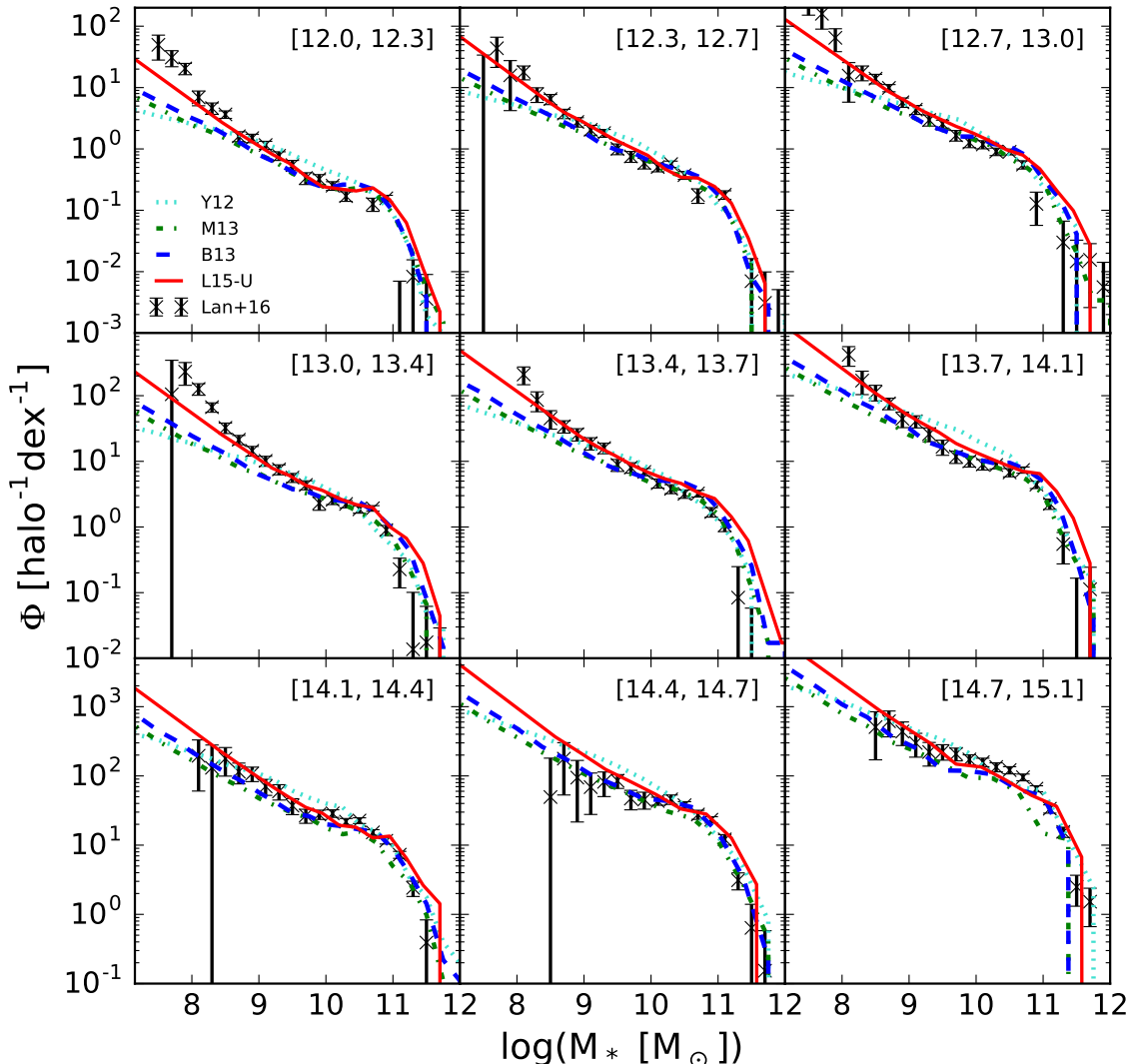
Figure 4. The observed (data points) and predicted (lines) conditional stellar mass functions of galaxies in groups of different halo masses, as indicated in individual panels.

to estimate the virial radius and velocity dispersion of the halo, which in turn are used to update the group membership. The procedure is iterated until both group memberships and halo masses converge for all groups. Yang et al. (2007) used mock catalogs constructed from N-body simulations to show that the dark matter halo masses estimated in this way are consistent with those directly obtained from the simulations, with scatter of ~ 0.3 dex over three orders of magnitude in halo masses that cover the mass range relevant to our analyses. When we compare the CSMFs obtained from models with the observational results, an uncertainty of ~ 0.3 dex is included in the model predictions. The halo masses used here are M_{200}, the total mass enclosed by a radius, r_{200}, within which the average density is 200 times the mean density of the universe.

    Lan et al. used only groups at $z < 0.05$, where halos with masses of $M_{200} > 10^{12} M_\odot$ are complete. To limit the uncertainty in redshifts due to peculiar velocities, they also eliminated groups at $z < 0.01$. With the groups and their

positions identified in the SDSS DR7 survey area, Lan et al. estimated the excess of galaxy number in each luminosity bin within a projected distance of r_{200} of each group. The conditional luminosity function (CLF) of galaxies is then obtained by averaging galaxy counts within all groups of a given halo mass, with subtractions of the background and projection effects due to clustering on large scales (see Lan et al. 2016, for the detail). Lan et al. applied this method to the photometric sample of SDSS DR7, down to a r-band model magnitude of 21. This corresponds to $M_r \approx -12$ (or $L \approx 10^7 L_\odot$) and $M_r \approx -14$ at $z = 0.01$ and 0.05, respectively. Since the number density of more massive halos is smaller, Lan et al. was able to estimate the CLF down to $M_r \sim -12$ for low-mass halos ($M_{200} \sim 10^{12} M_\odot$), but only to $M_r \sim -14$ for massive halos.

    To convert their CLFs into the corresponding CSMFs, we use a mass-to-light relation based on galaxy colors and luminosities (e.g. Bell et al. 2003) to obtain the stellar masses of galaxies. However, the uncertainty in the observed galaxy
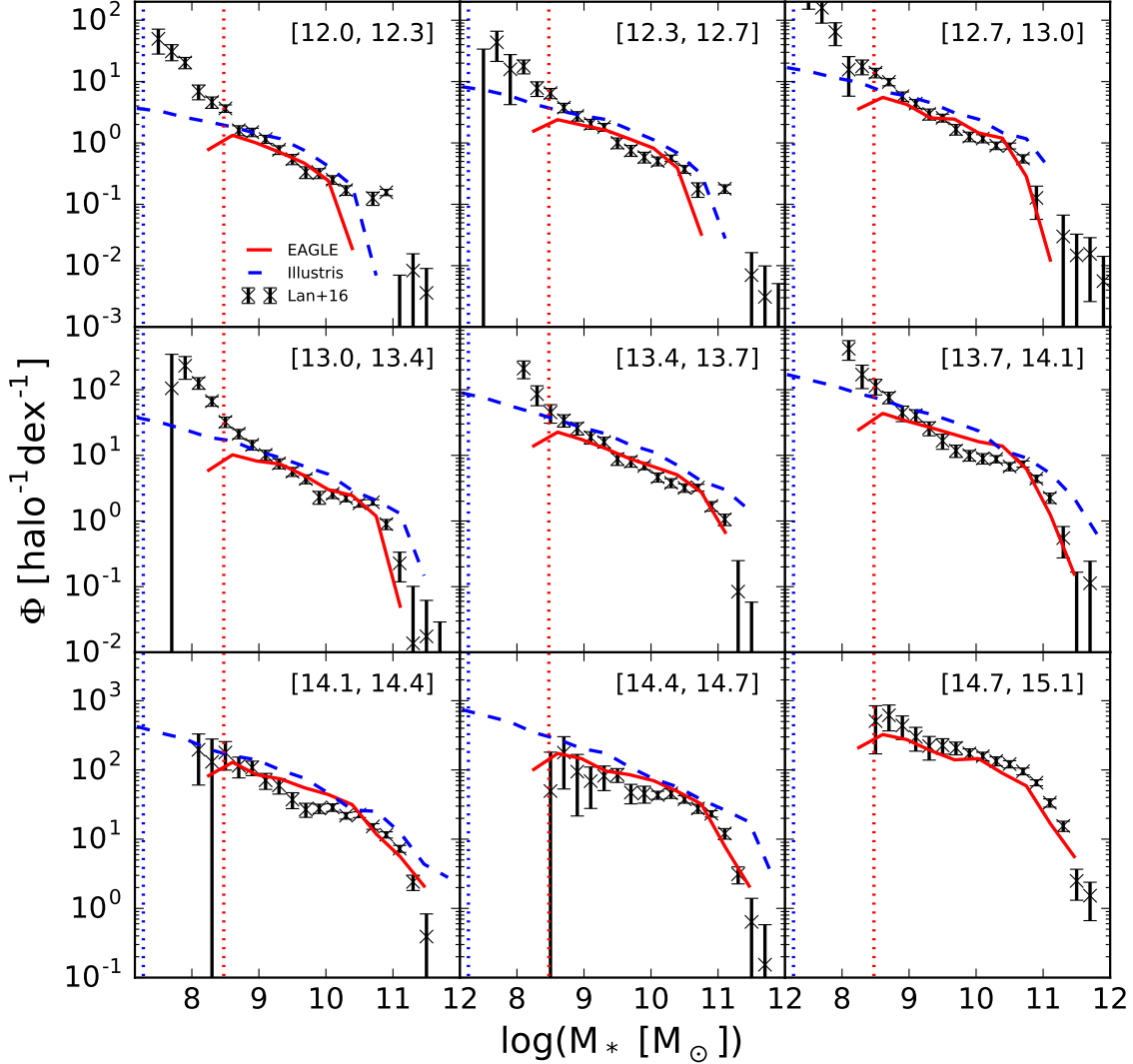
Figure 5. The comparison between the observed conditional stellar mass functions of galaxies (data points) with the results of EAGLE and Illustris simulations (lines), for groups of different halos masses, as indicated in each panel. The two vertical lines indicate the mass limits of the two simulations.

colors, especially for faint galaxies, may bias the stellar mass estimates and, therefore, the stellar mass functions. To reduce such bias, we first separate galaxies into blue and red populations by using the u-r color separation suggested by Baldry et al. (2004) [see their equation (11)]. We then use the observed luminosity of a galaxy and the mean u-r color for the galaxy population at that luminosity, instead of the observed color of the galaxy, to estimate the stellar mass. The mean u-r color-luminosity relations for the blue and red populations are derived in Lan et al. (2016) [their equations (C2) and (C3)] based on the same data set. We have made tests either by using the observed galaxy color or by artificially introducing some uncertainties in the galaxy color, and found that all these do not lead to any qualitative change of our results. Note again, as described in §2, our model predictions for the stellar masses of individual galaxies also include some uncertainties in the stellar mass estimates to

mimic the uncertainties in the observational stellar masses. Lan et al. adopted a Kroupa (2001) IMF for the CSMFs.

With the estimated stellar masses of individual galaxies, we measure the CSMFs using the same method Lan et al. did for the CLFs. The stellar mass functions are measured down to the limiting stellar masses at which both the stellar masses of blue and red galaxies derived from the flux limit photometric sample ($r < 21$) are complete. In addition, the limiting stellar mass bins are selected to ensure that they each contain at least five groups. We bootstrap the group catalog 200 times to estimate the errors in the derived CSMFs.

Figure 4 compares the CSMFs to those predicted by the empirical models. The predictions by the M13 and B13 models are qualitatively similar, with B13 predicting more low-mass galaxies. Both models under-predict the CSMFs at the low stellar mass ends, and the under-prediction is more significant for groups of lower halo masses. Only for massive
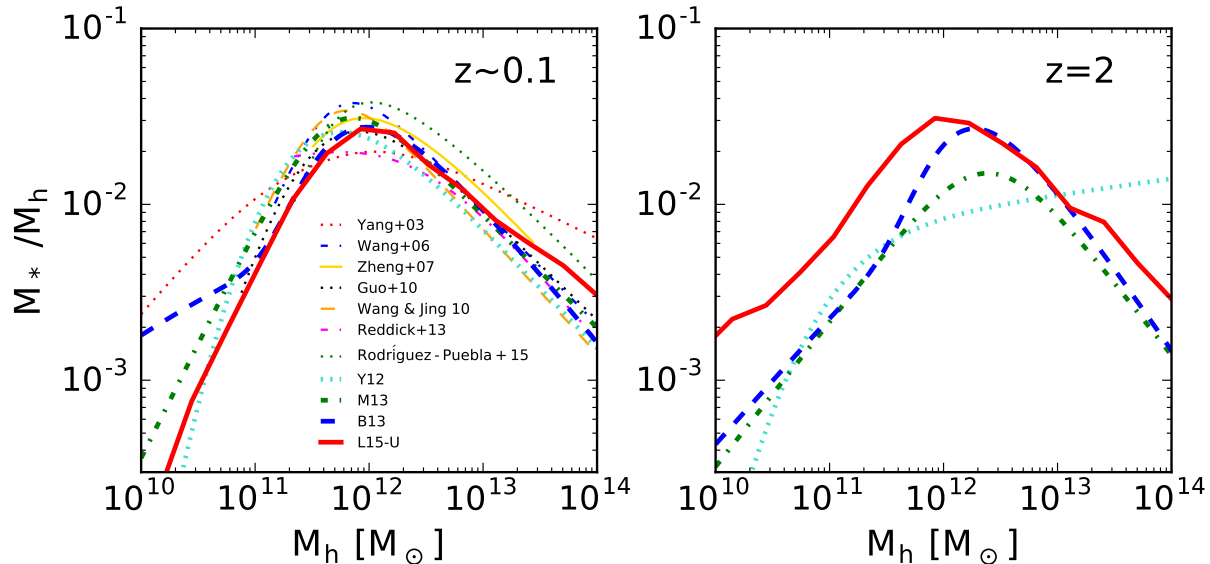
Figure 6. The average stellar mass - halo mass relation for central galaxies from the empirical models considered in this paper, along with the results in the literature from recent studies that adopted empirical approaches such as halo abundance matching, conditional luminosity function and halo occupation distribution, for local Universe (left) and $z = 2$ (right).

clusters are the predictions consistent with the observational data. The predictions of Y12 are too shallow in the low mass end; the model systematically under-predicts the CSMF at the low mass end and over-predicts that in the intermediate mass range. In particular, Y12 does not predict any upturn seen in the data.

The L15 model matches the overall behaviors of the CSMFs over the entire halo mass range. It also matches the CSMFs in detail for most of the halo mass bins. However, the low-mass upturn it predicts for more massive halos may be too steep, especially for the two most massive samples. As mentioned above, the L15 model used the composite CLF of galaxies in rich clusters given by Popesso et al. (2006) as one of the constraints on their model. The faint-end upturn in this composite CLF is significantly steeper than that of Lan et al. used here. The over-prediction is therefore due to the observational data which the model was tuned to match with. The model seems to under-predict the CSMF at the low-mass end in two mass bins: the lowest mass bin of $\log(M_h/M_\odot) = [12.01, 12.34]$, and the intermediate mass bin of $\log(M_h/M_\odot) = [13.03, 13.37]$. It is unclear if these discrepancies are due to random fluctuations in the data, or indicate that the L15 model has to be modified to accommodate the data. We will come back to this in the following section.

Figure 5 compares the observational data with the two gas simulations. Illustris simulation mismatches the observation over a wide range of stellar masses for almost all the halo mass bins. Overall, the simulation significantly under-predicts the CSMFs at the faint ends, and over-predicts them in both the massive and intermediate mass ranges. EAGLE simulation appears to be in better agreement with the observation, except that it does not reproduce sufficient number of massive galaxies in low-mass halos. Unfortunately, its mass resolution prevents us from probing its behavior at the faint end.

4   MODEL PREDICTIONS

In this section, we compare all the empirical models in their predictions for the stellar mass - halo mass relation, the star formation rates and stellar masses in halos of different masses at different redshifts, and for the SMFs of high-redshift galaxies.

4.1   Stellar mass - halo mass relation

Figure 6 shows the stellar mass - halo mass relation predicted by our updated model, in comparison with the predictions of the other three empirical models considered here and the results from the literature. Different models made different assumptions for conversions from luminosity to stellar mass, for prescription of scatter in the relation, and cosmological models. They also employed different observations as constraints for the models. Given all these differences, it is remarkable that the predictions of most models are consistent with each other within ~ 0.2 dex at $z \sim 0.1$ for a large range of halo masses. All models predict a characteristic mass scale, $M_h \sim 10^{12} M_\odot$, at which the stellar mass to halo mass ratio peaks. Among the more recent results, B13 is an exception in that it predicts a strong upturn at the low-mass end. The earlier result of Yang et al. (2003) was obtained by using their luminosity - halo mass relation together with the assumption of a constant stellar mass to luminosity ratio, $M/L = 1.8 \ M_\odot/L_\odot$ (in the b_J band of 2dFGRS which they used to constrain their model).

At higher redshift, however, the predictions by different empirical models differ significantly. In particular, the update of L15, L15-U, predicts a much higher star formation efficiency for low mass halos at high redshift, because of the boost of star formation rate at $z > z_c$ in low mass halos to match the upturns in the CSMFs.
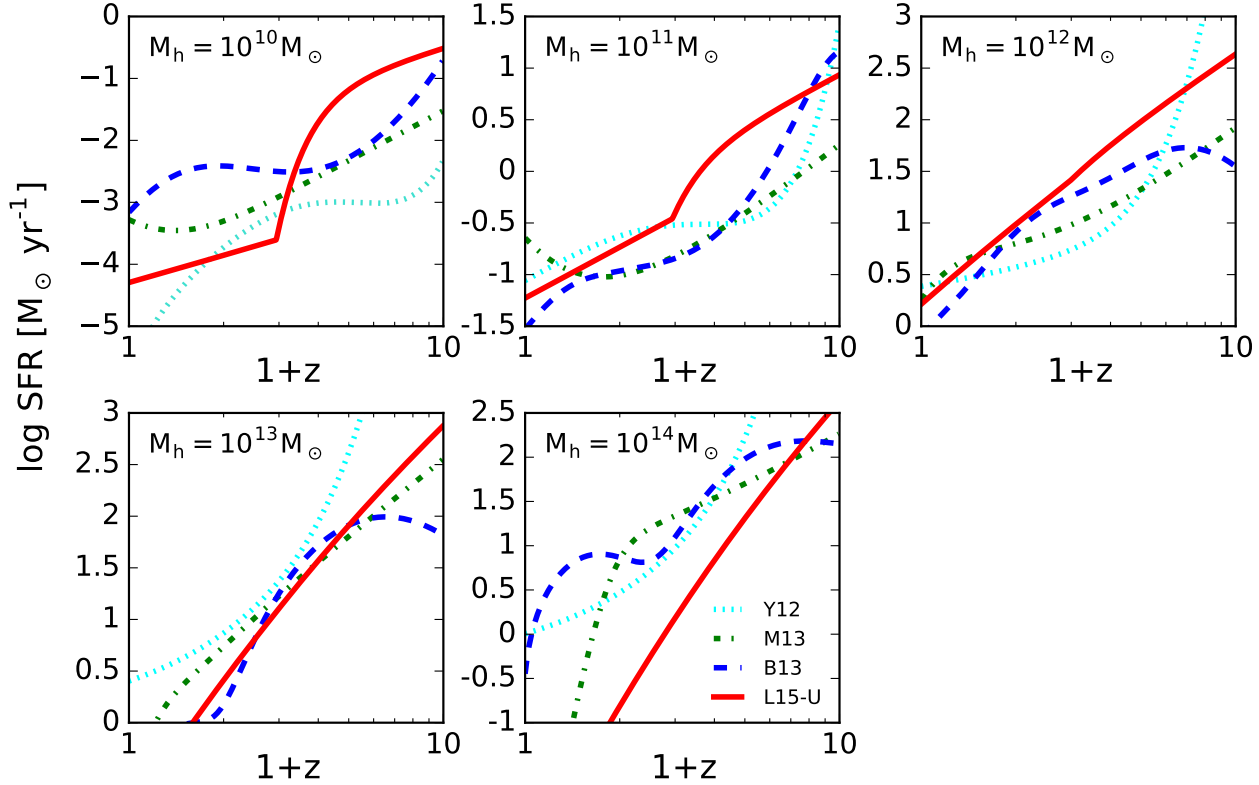
Figure 7. The average star formation rate of central galaxies as a function of redshift for halos of different masses, as predicted by various empirical models, as indicated.

4.2 Star formation histories in dark matter halos

Figure 7 compares the empirical models in terms of their predictions for the average star formation rate (SFR) of central galaxies in halos at different redshifts. Some models predict complicated star formation histories that are clearly due to over-fitting of the observational data. The L15-U model predicts much higher SFRs at $z \geqslant 2$ in low-mass halos than other models, which is clearly a consequence of the strong upturns at the faint-ends of the CSMFs used to constrain the model. The existence of a characteristic redshift, $z \sim 2$, is clearly seen in halos with $M_h < 10^{12}\,\mathrm{M}_\odot$, and its physical implications will be discussed later.

Figure 8 shows the model predictions for the average star formation histories of central galaxies in halos of different present-day masses. The predictions of different models are very different. In particular, for present-day dwarf galaxies that reside in halos of $M_h(0) < 10^{11}\mathrm{M}_\odot$, L15-U predicts a very active star formation episode at $z > 2$. In contrast, most of the stars in such halos are formed at $z < 2$ in all other models. This difference has other observational consequences. Indeed, as discussed in Lu et al. (2014) and Lu et al. (2015), the early starburst in low-mass halos predicted by L15 is consistent with the observations that a significant fraction of old stellar population exists in local dwarf galaxies (e.g. Weisz et al. 2011) and that the star formation rate function at the low-rate end is very steep at $z > 4$ (e.g. Smit et al. 2012). For Milky-Way sized halos, the star formation history predicted by L15-U is broader than those

predicted by the other three models. For massive halos with $M_h(0) \geqslant 10^{14}\mathrm{M}_\odot$, L15-U predicts a decline of the SFR with decreasing redshift starting from relatively high redshifts, in contrast to the predictions of B13 and Y12 that the star formation rates remain relatively high all the way to the present time, and to the prediction of M13 that a rapid decline only occurs at $z < 1$.

All these results demonstrate that different empirical models can make vastly different predictions for the star formation histories for present-day galaxies, even though all the models are tuned to match the observed SMFs.

4.3 Stellar mass assembly histories

Figure 9 shows the average stellar mass assembly histories for the central galaxies in halos of different present-day masses predicted by different models. The model predictions take into account *in situ* star formation, accretion of satellites, and stellar mass loss due to stellar evolution. Again, for low-mass halos, where the increase of stellar mass is dominated by *in situ* star formation (Lu et al. 2015), L15-U is distinct from the other models in that about half of their stellar mass at the present was already in place by $z \sim 2$ via star formation (see Figure 8).

For Milky-Way sized halos, however, the differences between the model predictions are milder. All the models predict that about half of stellar mass was in place by $z \sim 1$. There is a significant difference between L15-U and other
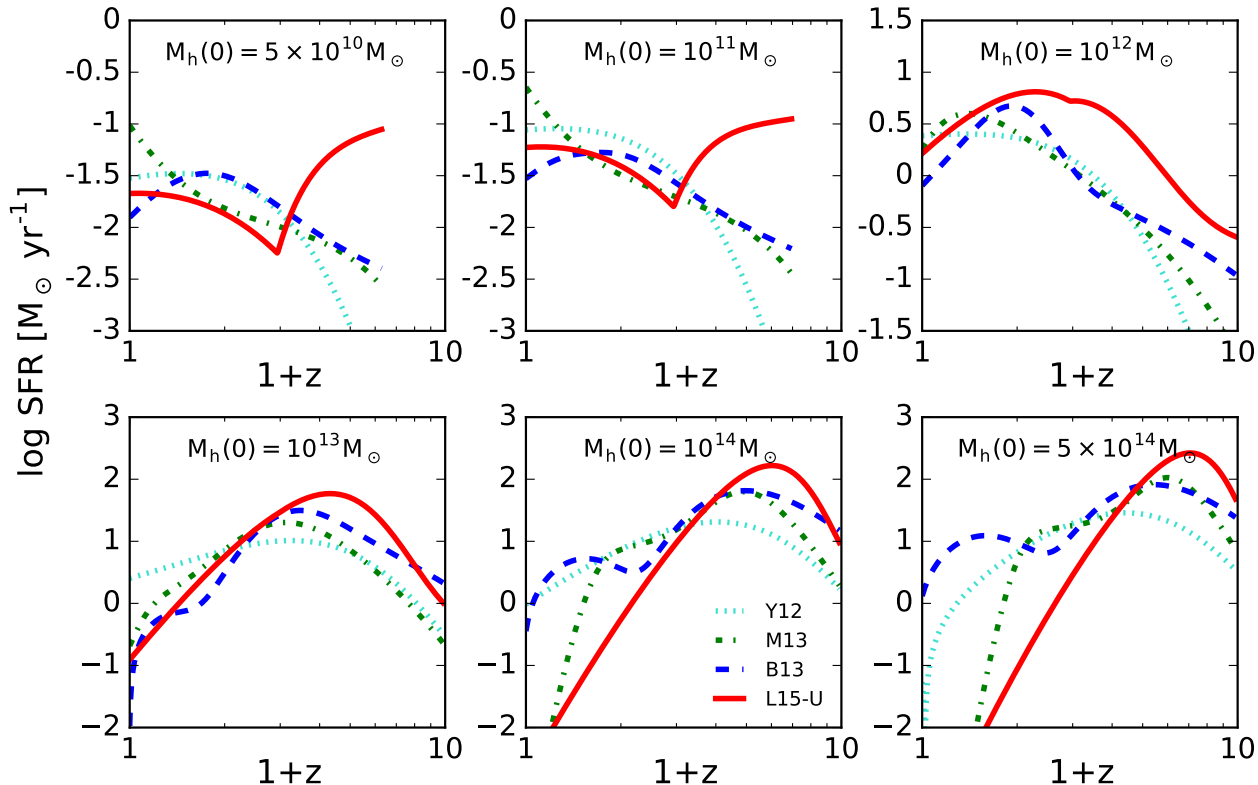
Figure 8. The average star formation rate of central galaxies as a function of redshift for halos of different present-day masses, predicted by the empirical models, as indicated.

models at high z. For example, L15-U predicts that about 15% of the final stellar mass was assembled by $z \sim 2$, while less than 10% was predicted by the other models.
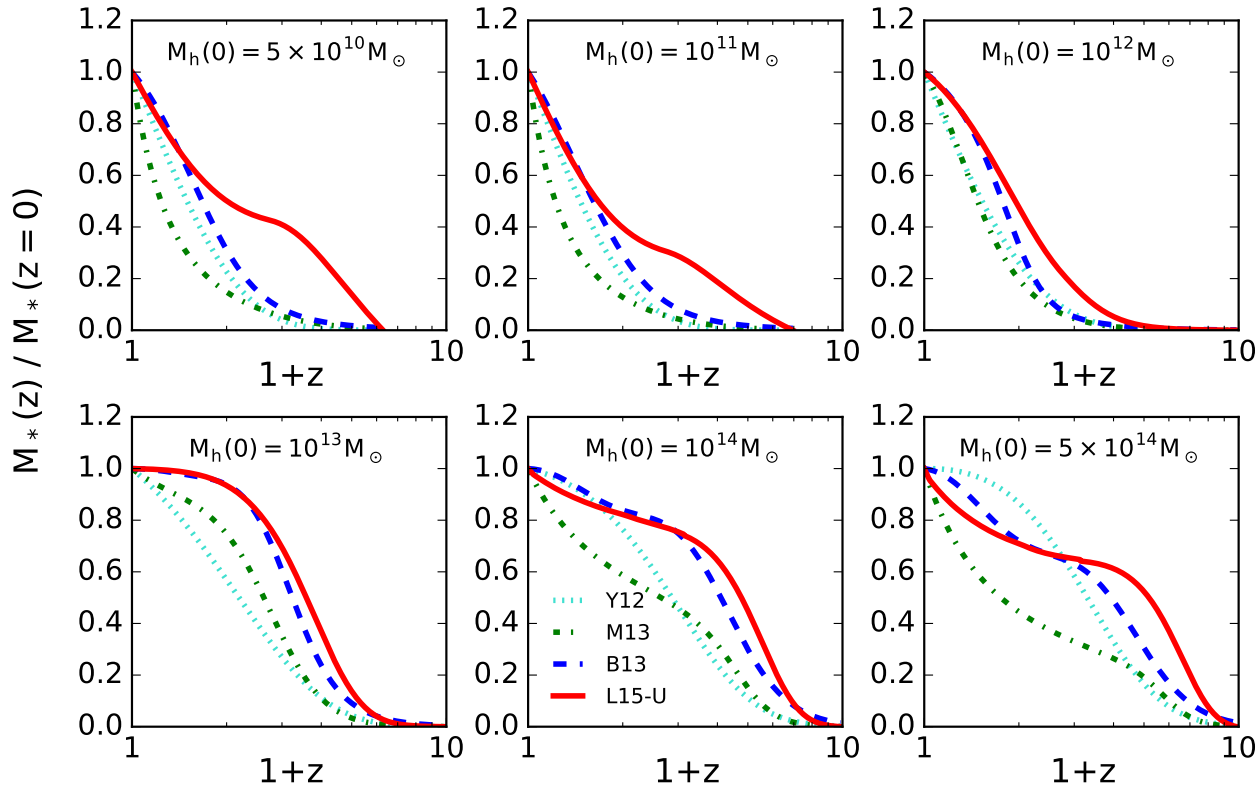
For central galaxies in present-day massive halos with $M_h(0) > 10^{14} M_\odot$, the predictions of different models again become very different. M13 predicts a much later assembly for these galaxies than any other models. The predictions of B13 look similar to L15-U, but the increase in stellar mass with time is due to different reasons. While L15-U predicts that the increase at $z < 2$ is dominated by accretion of stars from satellites, B13 predicts that a significant fraction of the increase at $z < 2$ is actually due to *in situ* star formation (see Figure 8). This difference is again due to the boost of star formation in low-mass halos at high z in the L15-U model. The increased amount of stars formed in progenitors at high z makes the accretion of stars more important in the growth of stellar mass in a massive galaxy, and the fraction of stars formed in situ has to be decreased proportionally in order to match the final stellar mass of the galaxy. The results demonstrate the importance of properly modeling the star formation in low-mass progenitors at high z in order to understand the star formation and stellar mass assembly histories of massive galaxies at the present day.

4.4 Stellar mass functions of high-redshift galaxies

Figure 10 shows the predictions of the empirical models for the stellar mass functions of galaxies at a number of red-

shifts. The predictions of B13 and M13 are similar in both slopes and amplitudes at the low mass ends, but B13 predicts many more massive galaxies than M13, particularly at high redshifts. Y12 predicts significantly flatter slopes at the low-mass ends, and more galaxies in the intermediate mass range, than the other three models. The stellar mass functions predicted by the L15-U model match the predictions of B13 at $M_* > 10^{10} M_\odot$, but are significantly steeper at the low-mass ends.

We select some observational SMFs of high redshift galaxies from the literature to compare with the model predictions. Specifically, we use the SMFs at $1.3 < z < 3.5$ given by Pérez-González et al. (2008) and Marchesini et al. (2009). Pérez-González et al. used a sample combining data in three different fields with a total area of 664 arcmin^2 that have a total $\sim 28,000$ systems selected with the $3.6 - 4.5\mu$m photometry of *Spitzer Space Telescope* (Werner et al. 2004). The sample is complete down to $M_* = 10^{10} M_\odot$. Marchesini et al. combined data from the deep NIR MUSYC, the ultra-deep FIRES, and the GOODS-CDFS surveys to derive the SMFs from the optical to MIR broad bands photometry. Pérez-González et al. assumed a Salpeter (1955) IMF while Marchesini et al. adopted a pseudo-Kroupa (2001) IMF. It is known that the stellar mass estimated using a Salpeter IMF is roughly a factor of 1.4 higher than that given by a pseudo-Kroupa or Chabrier IMF, and we correct all the stellar masses to the IMF we adopt here. For the SMFs at even higher redshifts, $z = 4 - 5$, we use the results by Lee

Figure 9. The average stellar mass assembly history of central galaxies as a function of redshift for halos of different present-day masses, predicted by various empirical models as indicated.

et al. (2012) and Song et al. (2016). Both B13 and L15-U match the observational data well at $M_* > 10^9 \mathrm{M}_\odot$, while the other two models match the high-z data poorly at the high-mass end. The prediction of the L15-U is significantly steeper than the observational results given by Song et al. at $z > 4$. If the high-z SMFs are as shallow as those given by Song et al., then there may be a tension between the observed CSMFs at low z and the observed SMFs at high z, at least within the model family represented by the halo-based empirical model of L15.

5   SUMMARY AND DISCUSSION

Galaxy formation and evolution within the current cosmological frame are controlled by a number of physical processes, many of which are still poorly understood from first principles. In the absence of a proper understanding of these processes, halo-based empirical models provide a useful way to establish the link between galaxies and CDM halos purely on the basis of observations and the current cosmology. In this paper we use a variety of galaxy stellar mass functions to test a number of popular empirical models. In particular, we focus on using the conditional stellar mass functions (CSMFs) of galaxies in galaxy groups as obtained by Lan et al. (2016) to test the models. We find that the CSMFs predicted by different models can be very different, even though they are all tuned to match the observed stellar mass function of the total galaxy population. This clearly

demonstrates the power of the CSMFs in constraining models. Since the CSMFs are measured from observations in the nearby Universe, the samples that can be used are larger, and the stellar mass functions can be measured to the low-mass ends. As the galaxies that reside in present-day galaxy systems, such as clusters and groups of galaxies, are expected to have formed at various redshifts, the CSMFs in groups/halos of different masses carry important information about galaxy formation in dark matter halos at different redshifts.

The CSMFs are then used as constraints to update the original model by Lu et al. (2014, 2015). The model parameters obtained here are very similar to those obtained in the original paper which uses a completely different set of observational constraints, demonstrating that the different data sets are consistent with each other. The observational constraints clearly prefer a model in which star formation in low-mass halos changes behavior at a characteristic redshift $z_c \sim 2$. There is also a tentative evidence that this characteristic redshift depends on environments, becoming $z_c \sim 4$ in regions that eventually evolve into rich clusters of galaxies. However, given the uncertainties of the current observed CSMFs in the low-mass ends, this environmental dependence of z_c needs to be confirmed with better data.

We compare the predictions of a number of popular halo-based empirical models and two numerical simulations of galaxy formation. We find that the two numerical simulations fail to match the observational data one way or
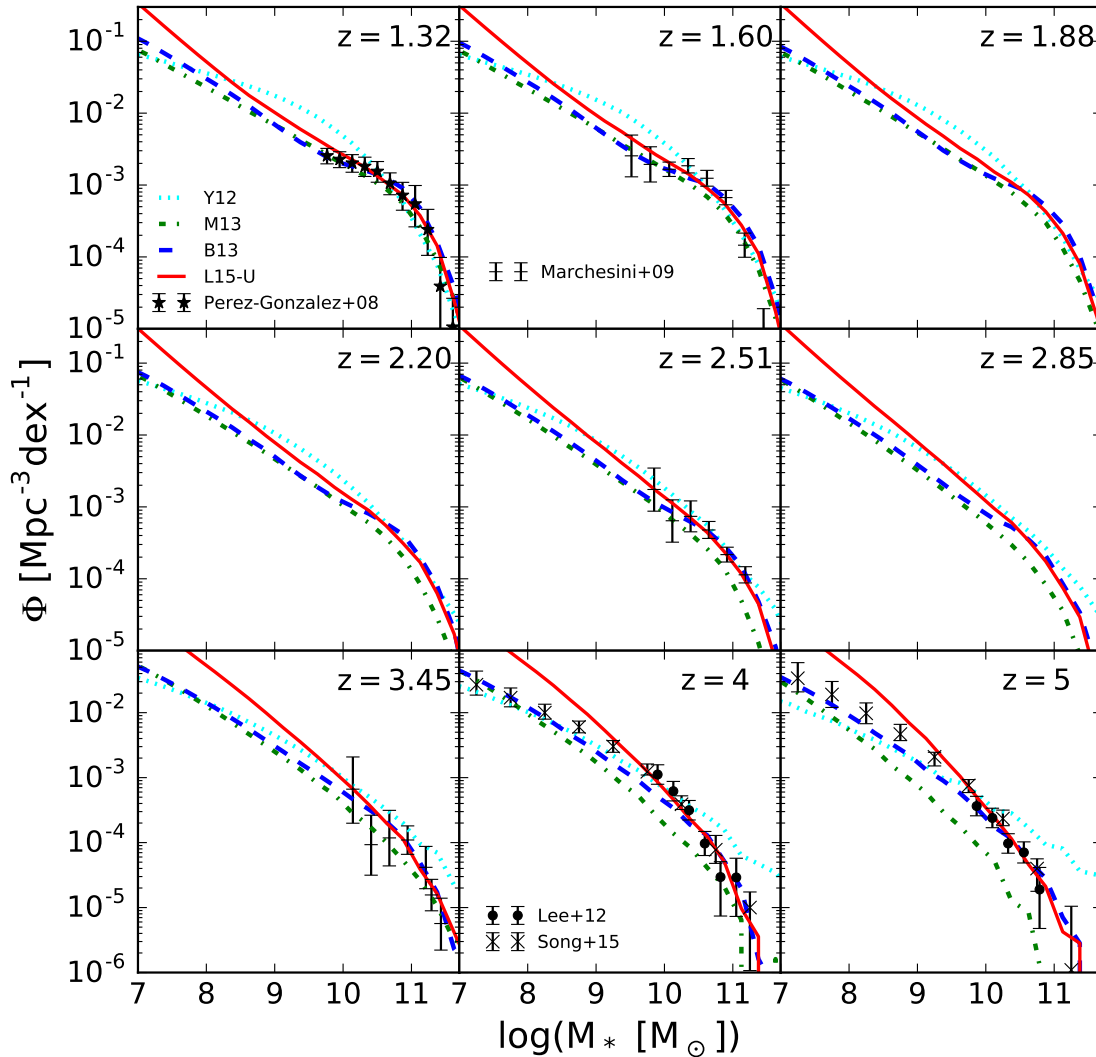
Figure 10. The model predictions for the field stellar mass functions at high redshifts (solid) in comparison with observations.

another. The empirical models by Yang et al. (2012) and Moster et al. (2013) fail to reproduce the faint-end upturn of the field SMFs from observations. The model by Behroozi et al. (2013) reproduces the faint-end upturn, but it is a combined result of over-prediction for central galaxies and under-prediction for satellites at the faint-end. In contrast, the model by Lu et al. (2014, 2015) matches reasonably well the CSMFs in halos of different masses. The Lu et al. model predicts a much higher star formation efficiency than the other models for low-mass halos at redshifts higher than a characteristic redshift after which the star formation is suppressed.

We use our constrained model to make predictions for a number of statistical properties of the galaxy population. These include the stellar mass functions of galaxies at high z, the stellar mass - halo mass relations at different redshifts, and the star formation and stellar mass assembly histories of galaxies in dark matter halos of different masses. A comparison of our model predictions with those of other empirical models shows that different models can make vastly

different predictions for these properties, even though all of them are tuned to match the observed stellar mass functions of galaxies. In particular, our constrained model predicts a much higher *in situ* star formation rate at $z \geqslant 2$ for present-day dwarf galaxies than the other models. As a result, such galaxies have about 40% of their current-day stellar mass already in place by $z \sim 2$. Because of this boosted star formation in low-mass halos at high z, the role of accretion of stars from satellite galaxies, relative to *in situ* star formation, in the build up of massive galaxies is more important in our model than in the other models.

One of the main predictions of our constrained model is the existence of a characteristic redshift that separates an active star formation phase from a subdued star formation phase in low-mass halos. This change in star formation mode is likely related to the feedback processes that regulate star formation. As discussed in Lu et al. (2014, 2015), energy feedback from stars and AGNs associated with active star formation and super-massive black hole accretion at high redshift may preheat the gas media around dark matter ha-

los and suppress gas accretion and star formation at lower redshift (Mo & Mao 2002, 2004). Based on plausible assumptions about the star formation histories of the universe and the density of the intergalactic medium, the pre-heating is expected to occur around $z = 2 - 3$, and the specific entropy of the preheated gas is $\sim 10 \mathrm{KeVcm}^2$, which is important in affecting star formation in low-mass halos, because of their relatively shallow gravitational potential wells, but has no significant effects on halos with masses above $\sim 10^{12} \, \mathrm{M_\odot}$ (e.g. Lu & Mo 2007). This preheating may also explain why the cold gas mass function at $z \sim 0$ is shallow (Mo et al. 2005). In such a scenario, the pre-heating is expected to occur earlier in regions occupied by present-day massive halos, because intensive star formation and AGN activity are expected to occur earlier in higher density regions where gravitational collapse is more accelerated. Our tentative finding of the positive dependence of the characteristic redshift on halo mass is in agreement with such an expectation, but better observational data are needed in order to examine such dependence in more detail.

REFERENCES

Abazajian K. N. et al., 2009, ApJS, 182, 543
Baldry I. K. et al., 2004, ApJ, 600, 681
Baldry I. K., Glazebrook K., Driver S. P., 2008, MNRAS, 388, 945
Baldry I. K. et al., 2012, MNRAS, 421, 621
Behroozi P. S., Conroy C., Wechsler R. H., 2010, ApJ, 717, 379
Behroozi P. S., Wechsler R. H., Conroy C., 2013, ApJ, 770, 57
Bell E. F., McIntosh D. H. Katz, N., Weinberg M. D., 2003, ApJS, 149, 289
Berlind A. A., Weinberg D. H., 2002, ApJ, 575, 587
Blanton M. R. et al., 2003, ApJ, 592, 819
Blanton M. R. et al., 2005, AJ, 129, 2562
Bower R. G., Benson A. J., Malbon R., Helly J. C., Frenk C. S., Baugh C. M., Cole S., Lacey C. G., 2006, MNRAS, 370, 645
Bruzual G., Charlot S., 2003, MNRAS, 344, 1000

Bullock J. S.,Wechsler R. H., Somerville R. S., 2002, MNRAS, 329, 246
Chabrier G., 2003, PASP, 115, 763
Charlot S., Fall S. M., 2000, ApJ, 539, 718
Cole S. et al., 2001, MNRAS, 326, 255
Conroy C., Wechsler R. H., Kravtsov A. V., 2006, ApJ, 647, 201
Conroy C., Gunn J. E., White M., 2009, ApJ, 699, 486
Croton D. J. et al., 2006, MNRAS, 365, 11
Dekel A., Silk J., 1986, ApJ, 303, 39
Dubois Y. et al., 2014, MNRAS, 444, 1453
Fall S. M., Efstathiou G., 1980, MNRAS, 193, 189
Feroz F., Hobson M. P., Bridges, M., 2009, MNRAS, 398, 1601
Ferrarese L., Merritt D., 2000, ApJ, 539, 9
Gallazzi A., Charlot S., Brinchmann J., White S. D. M., Tremonti C. A., 2005, MNRAS, 362, 41
Governato F. et al., 2004, ApJ, 607, 688
Governato F. et al., 2010, Nature, 463, 203
Guedes J., Callegari S., Madau P., Mayer L., 2011, ApJ, 742, 76
Guo Q., White S., Li C., Boylan-Kolchin M., 2010, MNRAS, 404, 1111
Guo Q. et al., 2011, MNRAS, 413, 101
Jiang F., van den Bosch F. C., 2014, MNRAS, 440, 193
Jing Y. P., Mo H. J., Borner G., 1998, ApJ, 494, 1
Kauffmann G., Colberg J. M., Diaferio A., White S. D. M., 1999, MNRAS, 303, 188
Kauffmann G. et al., 2003, MNRAS, 341, 33
Kang X., Jing Y. P., Mo H. J., Börner G., 2005, ApJ, 631, 21
Kereš D., Katz N., Weinberg D. H., Davé R., 2005, MNRAS, 363, 2
Kereš D., Katz N., Fardal M., Davé R., Weinberg D. H., 2009, MNRAS, 395, 160
Khandai N., Di Matteo T., Croft R., Wilkins S. M., Feng Y., Tucker E., DeGraf C., Liu M. S., 2015, MNRAS, 450, 1349
Kroupa P., 2001, MNRAS, 322, 231
Kravtsov A. V., Gnedin O. Y., Klypin A. A., 2004, ApJ, 609, 482
Lan T.-W., Ménard B., Mo H. J., 2016, MNRAS, 459, 3998
Lee K.-S. et al., 2012, ApJ, 752, 66
Li C., White S. D. M., 2009, MNRAS, 398, 2177
Lu Y., Mo H. J., 2007, MNRAS, 377, 617
Lu Y., Kereš D., Katz N., Mo H. J., Fardal M., Weinberg, M. D., 2011, MNRAS, 416, 660
Lu Y., Mo H. J., Katz N., Weinberg M. D., 2012, MNRAS, 421, 1779
Lu Z., Mo H. J., Lu Y., Katz N., Weinberg M. D., van den Bosch F. C., Yang X., 2014, MNRAS, 439, 1294
Lu Z., Mo H. J., Lu Y., Katz N., Weinberg M. D., van den Bosch F. C., Yang X., 2015, MNRAS, 450, 1604
Marchesini D., van Dokkum P. G., Förster Schreiber N. M., Franx M., Labbé I., Wuyts S., 2009, ApJ, 701, 1765
Martin D. C. et al., 2005, ApJL, 619, L1
McConnell N. J., Ma C. P., Gebhardt K., Wright S. A., Murphy J. D., Lauer T. R., Graham J. R., Richstone D. O., 2011, Nature, 480, 215
Mo H. J., Mao S., White S. D. M., 1998, MNRAS, 295, 319
Mo H. J., Mao S., White S. D. M., 1999, MNRAS, 303, 175
Mo H. J., Mao S., 2002, MNRAS, 333, 768

Mo H. J., Mao S., 2004, MNRAS, 353, 829

Mo H. J., Yang X., van den Bosch F. C., Katz N., 2005, MNRAS, 363, 1155

Mo H. J., van den Bosch F. C., White S. D. M., 2010, Galaxy Formation and Evolution. Cambridge University Press, New York, NY

Moustakas J., et al., 2013, ApJ, 767, 50

Moster B. P., Somerville R. S., Maulbetsch C., van den Bosch F. C., Macciò A. V., Naab T., Oser L., 2010, ApJ, 710, 903

Moster B. P., Naab T., White S. D. M., 2013, MNRAS, 428, 3121

Nelson D., Genel S., Vogelsberger M., Springel V., Sijacki D., Torrey P., Hernquist L., 2015, MNRAS 448, 59

Okamoto T., Eke V. R., Frenk C. S., Jenkins A., 2005, MNRAS, 363, 1299

Panter B., Jimenez R., Heavens A. F., Charlot S., 2007, MNRAS, 378, 1550

Parkinson H., Cole S., Helly J., 2008, MNRAS, 383, 557

Peacock J. A., Smith R. E., 2000, MNRAS, 318, 1144

Pérez-González P. G. et al., 2008, ApJ, 675, 234

Planck Collaboration et al., 2014, A&A, 571

Popesso P., Biviano A., Bhringer H., Romaniello M., 2006, A&A, 445, 29

Reddick R. M., Wechsler R. H., Tinker J. L., Behroozi P. S., 2013, ApJ, 771, 30

Rodríguez-Puebla A., Avila-Reese V., Yang X., Foucaud S., Drory N., Jing Y. P., 2015, ApJ, 799, 130

Salpeter E. E., 1955, ApJ, 121, 161

Schaye J. et al., 2015, MNRAS 446, 521

Sheth R. K., Mo H. J., Tormen, G., 2001, MNRAS, 323, 1

Skilling J., 2006, Bayesian Analysis, 1, 833

Skrutskie M. F. et al., 2006, AJ, 131, 1163

Smit R., Bouwens R. J., Franx M., Illingworth G. D., Labbe I., Oesch P. A., van Dokkum P. G., 2012, ApJ, 756, 14S

Somerville R. S., Hopkins P. F., Cox T. J., Robertson B. E., Hernquist L., 2008, MNRAS, 391, 481

Song M. et al., 2016, ApJ, 825, 5

Vale A., Ostriker J. P., 2004, MNRAS, 353, 189

Vale A., Ostriker J. P., 2006, MNRAS, 371, 1173

van den Bosch F. C., Yang X., Mo H. J., 2003, MNRAS, 340, 771

van den Bosch F. C., Jiang F., Hearin A., Campbell D., Watson D., Padmanabhan N., 2014, MNRAS, 445, 1713

Vogelsberger M. et al., 2014, Nature, 509, 177

Wang L., Li C., Kauffmann G., De Lucia G., 2006, MNRAS, 371, 537

Wang L., Jing Y. P., 2010, MNRAS, 402, 1796

Weisz D. R. et al., 2011, ApJ, 739, 5

Werner M. W. et al., 2004, ApJS, 154, 1

White S. D. M., Rees M. J., 1978, MNRAS, 183, 341

White S. D. M., Frenk C. S., 1991, ApJ, 379, 52

White M., 2001, MNRAS, 321, 1

Wright E. L. et al., 2010, AJ, 140, 1868

Yang X., Mo H. J., van den Bosch F. C., 2003, MNRAS, 339, 1057

Yang X., Mo H. J., van den Bosch F. C., Jing Y. P., 2005, MNRAS, 356, 1293

Yang X., Mo H. J., van den Bosch F. C., Pasquali A., Li C., Barden M., 2007, ApJ, 671, 153

Yang X., Mo H. J., Zhang Y., van den Bosch F. C., 2011, ApJ, 741, 13

Yang X., Mo H. J., van den Bosch F. C., Zhang Y., Han J., 2012, ApJ, 752, 41

Zehavi I. et al., 2004, ApJ, 608, 16

Zehavi I. et al., 2011, ApJ, 736, 59

Zhao D. H., Mo H. J., Jing Y. P., Börner G., 2003, MNRAS, 339, 12

Zheng X. Z., Bell E. F., Papovich C., Wolf C., Meisenheimer K., Rix H.-W., Rieke G. H., Somerville R., 2007, ApJ, 661, L41

Zhao D. H., Jing Y. P., Mo H. J., Börner G., 2009, ApJ, 707, 354